RSC Advances

ROYAL SOCIETY OF CHEMISTRY

www.rsc.org/advances

Simultaneous determination of two flavonoids based on disulfide linked β-cyclodextrin dimer and Pd clusters functionalized graphene-modified electrode

Xin Ran[a, 1], Long Yang[a, 1], Genfu Zhao[a], Hanzhang Ye[a], Yanqiong Zhang[a], Shuangmei Fan[a], Xiaoguang Xie[a, *], Hui Zhao[b, *], Can-Peng Li[a, *]

[a] School of Chemical Science and Technology, Yunnan University, Kunming 650091, PR China.

[b] Laboratory for Conservation and Utilization of Bio-resource, Yunnan University, Kunming 650091, PR China.

[1]These authors contributed equally to this work.

* Corresponding authors.

Fax or Tel: 86-871-65031119. E-mail: xgxie@ynu.edu.cn (X. xie); zhaohyau@yahoo.com.cn (H. Zhao); lcppp1974@sina.com (C.-P. Li)

Abstract: In the present work, ultrafine Pd clusters with a uniform size of ~2.0 nm were monodispersed on the surface of reduced graphene oxide (RGO) using a clean and green approach in the absence of additional reductants and surfactants. Disulfide linked β-cyclodextrin dimer (SS-β-CD) was non-covalently bonded to the surface of Pd@RGO. By combining the merits of Pd@RGO and the SS-β-CD, a highly sensitive electrochemical sensing platform was developed based on the SS-β-CD-Pd@RGO nanohybrids. Electrochemical simultaneous detection of baicalin and luteolin using SS-β-CD-Pd@RGO nanohybrids-modified electrode is described for the first time. The SS-β-CD showed higher supramolecular recognition capability than the native β-CD, which may be caused by the cooperative binding abilities of two adjacent CD units. Due to the synergistic effects from the Pd@RGO (*e.g.* the good electrochemical properties and large surface area) and SS-β-CD (*e.g.* a hydrophilic external surface, a high supramolecular recognition, and a good enrichment capability), the SS-β-CD-Pd@RGO modified electrode was found to have linear response ranges of 0.02–20.00 μM for baicalin and 0.01–10.00 μM for luteolin with relatively low detection limits of 0.0052 μM for baicalin and 0.0070 μM for luteolin, respectively. The results indicated that SS-β-CD-Pd@RGO nanohybrids are excellent sensing materials for the electrochemical determination of flavonoids. The proposed method could be successfully utilized to detect baicalin and luteolin in serum samples, and exhibited a promising application in practice.

1. Introduction

Flavonoids, plant polyphenolic compounds abundant in fruits and vegetables, exhibit a wide variety of biochemical and pharmacological effects, including antioxidant free-radical scavenging, anti-inflammatory, anti-carcinogenic, etc. [1] In plants, they are utilized in response to microbial infection. However, in animals and humans, flavonoids protect cells against damage caused by reactive oxygen species. [2] Moreover, they have the capacity to inhibit the growth of a wide range of bacteria via disruption of bacterial cell walls following by their complexation with the extracellular soluble protein components. [3] Flavonoids also exert anti-viral actions due to their favourable oxidation potentials. [4] Baicalin (**Scheme 1A**) and luteolin (**Scheme 1B**), belonging to the class flavonoids, are two important anti-inflammatory and anticancer drugs, which are widely used in medical practice. As a result of the above pharmacological effects, different kinds of concentrated composite herbal preparations that contain baicalin and luteolin as the active component have been used clinically as therapeutical medicine. Besides, a lot of health functional foods and different beverages usually contain baicalin and luteolin. Therefore, establishment of highly sensitive analytical techniques for the determination of baicalin and luteolin is of great significance in clinics, pharmaceutics, and functional foods. So far, several methods such as thin layer chromatography, [5] capillary electrophoresis, [6,7] GC, [8,9] HPLC, [10-12] fluorimetry, [13] and LC–MS [14,15] have been developed for the analysis of baicalin and luteolin. Although these methods have advantages of sensitivity and accuracy, their high cost and complicated operation limit their extensive application. Electrochemical detection is an attractive alternative to these techniques because it

features high sensitivity, instrument simplicity, fast response, low cost, and feasibility of miniaturization. Although the electrochemical methods have been reported for determination of the different type of flavonoids, [16-21] to the best of our knowledge, there are no reports yet for simultaneous determination of baicalin and luteolin by an electrochemical method.

Noble metals with ultrafine sizes have attracted considerable attention because of their large surface areas and high number of edge and corner atoms that enhance the catalytic properties of noble metal nanocomposites. [22,23] Therefore, the synthesis of small metal particles with high accessible surface areas is a worthwhile endeavor. Unfortunately, surface energies increase with decreased noble metal particle size, leading to serious aggregation of small particles. [24,25] Particularly, the synthesis of small sized particles with the sizes of less than 2 nm, which are also known as clusters differentiating from nanoparticles (NPs) due to their small sizes and narrow size distribution, represents many more challenges because of its high requirement of control over the nucleation and growth processes compared with that of NPs. [26,27] Thus, the metal particles were usually anchored to suitable supports to overcome the aggregation. [27,28] Graphene, which is a robust 2D sheet of sp^2-hybridized carbon, is the most promising one among all the available support materials. [29] Pd cluster and its composite are widely used for many applications because of their lower cost than other noble metals. [30] Research based on first-principles calculations indicates that Pd could interact with and bind more strongly to graphene because more interaction states and transmission channels are generated between them and because Pd tends to

grow into three-dimensional structures on graphene surfaces. [25] This provides a hint that graphene could be an ideal substrate for growing and anchoring Pd clusters for high-performance electrocatalytic or electrochemical devices.

Supramolecular host–guest recognition based on noncovalent interaction has attracted great attention in nowadays, which has been widely employed to develop different electrochemical sensors by modifying organic macrocyclic hosts on various electrodes. [18,31-38] Cyclodextrins (CDs), as the typical macrocyclic molecules, are oligosaccharides composed of six, seven, or eight glucose units (α-, β-, γ-CD, respectively), which are toroidal in shape with a hydrophobic inner cavity and a hydrophilic exterior and are capable of forming inclusion complexes with a wide variety of hydrophobic guests. [39,40] Graphene is a material that holds great promise for potential applications in many technological fields because of its high surface area, low cost, and high conductivity. [36,39] It has been reported that the composites of CDs and graphene could be formed by van der Waals force, hydrogen-bonding, and hydrophobic interaction. [34,37,39] A graphene that is functionalized with CDs is likely to obtain new functionalized materials that simultaneously possess the unique properties of graphene (*e.g.* high electrical conductivity and large surface area) and CDs (*e.g.* high supramolecular recognition and good enrichment capability). Thus, the integration of graphene and CDs can be potentially applied in the field of electrochemical sensing or biosensing. As a recently developing family of CD derivatives, bridged bis(β-CD)s exhibit significantly enhanced binding abilities and molecular recognition through the cooperative binding of two adjacent CD units in

comparison with native CDs. [41,42] Therefore, considerable efforts have been devoted in this field to design and synthesize various CD dimers with considerable structural diversity to achieve the enhanced binding abilities. [43] Hence, diverse functional groups such as organoseleniums, [44] disulfides, [45] pyridines, [46,47] ethylene glycol, [48] aromatic diamine, [49] and pyrene [50] have been used as the linker between two CD units. Unexpectedly, their molecular recognition behaviors have not been extensively investigated. In addition, these bridged bis(β-CD)s are rarely employed to construct electrochemical sensing or biosensing platforms.

In the present paper, ultrafine Pd clusters with a uniform size of ~2.0 nm were monodispersed on the surface of reduced graphene oxide (RGO) using a clean and green approach in the absence of additional reductants and surfactants. The disulfide linked β-cyclodextrin dimer (SS-β-CD) was non-covalently bonded to the surface of Pd@RGO. By combining the merits of Pd@RGO and the SS-β-CD, a highly sensitive electrochemical sensing platform was developed based on the SS-β-CD-Pd@RGO nanohybrids. The designed electrochemical sensing platform is illustrated in **Scheme 2**. Two flavonoid compounds, namely, baicalin and luteolin were chosen as simultaneous probes to verify the performance of the SS-β-CD-Pd@RGO nanohybrids.

2. Materials and methods

2.1 Chemicals

Graphite oxide was purchased from Nanjing XFNANO Materials Tech Co., Ltd.

(Nanjing, China). $PdCl_2$ and β-CD were obtained from Sigma Chemical Co. (St. Louis, MO, USA). Thiol-β-cyclodextrin (SH-β-CD) was purchased from Shandong Binzhou Zhiyuan Bio-Technology Co., Ltd (Shandong, China). Baicalin and luteolin were obtained from Aladdin Chemical Reagent Lo., Ltd. All aqueous solutions were prepared with deionized water (DW, 18 MΩ cm). All other reagents were of analytical grade.

2.2 Apparatus

Electrochemical impedance spectroscopy (EIS) and differential pulse voltammetery (DPV) experiments were performed with a CHI 660E Electrochemical Workstation from Shanghai Chenhua Instrument (Shanghai, China) and conducted using a three-electrode system, with the modified GCE as working electrode, a platinum wire as the counter electrode, a saturated calomel electrode (SCE) as the reference electrode. The morphologies of the prepared samples were characterized by a QUNT200 scanning electron microscopy (SEM, USA) and a JEM 2100 transmission electron microscopy (TEM, Japan). UV–visible spectra were analyzed in a U-2001 Hitachi (Tokyo, Japan) UV spectrophotometer. Fourier transform infrared (FTIR) study was performed over the wavenumber, range of 4000–400 cm^{-1} by a Thermo Fisher SCIENTIFIC Nicolet IS10 (Thermo Fisher, Massachusetts, USA) FTIR impact 410 spectrophotometer using KBr pellets. Thermogravimetric analysis (TGA) was carried out on a Q50 TGA (TA Instruments, New Castle, DE, USA), at a heating rate of 5 ^{o}C min^{-1} from 25 to 800 ^{o}C in argon.

155

156 **2.3 UV-vis spectroscopic measurements**

157 Inclusion complexes formation of baicalin/SS-β-CD, baicalin/β-CD,
158 luteolin/SS-β-CD, and luteolin/β-CD were studied in DW using the spectral shift
159 method. The concentration of baicalin and luteolin were kept constant at 50 μM, the
160 SS-β-CD concentration was 0.36 mM, while the β-CD concentration was 0.72 mM.
161 Initially, stock solutions of baicalin, luteolin, SS-β-CD, and β-CD in DW were
162 prepared. Aliquots from each solution were transferred to a 25 mL volumetric flask
163 and the volume was made up using DW so that the required concentrations are
164 obtained. The prepared solutions were stirred for 30 min at room temperature, filtered
165 through 0.45 μm membrane filter, and the UV-vis absorption spectra were recorded in
166 the wavelength range from 200 to 500 nm against blank solutions containing the same
167 concentrations of SS-β-CD or β-CD. The recorded spectra were compared to the
168 spectrum of free baicalin or luteolin.

169

170 **2.4 Preparation of the RGO**

171 The graphite oxide was exfoliated in to graphene oxide (GO) sheets by
172 ultrasonication at room temperature for 1 h. The as-obtained yellow-brown aqueous
173 suspension of GO was stored at room temperature and used for further experiment.
174 Compared with the traditional procedure using highly toxic hydrazine as reductant, a
175 green approach was adopted to prepare RGO reported by Fan et al. [51] with some
176 modifications. In a typical experiment, the pH of 50.0 mL of 0.5 mg mL^{-1} GO

aqueous suspension was adjusted to 11.0 using 1.0 M NaOH. Then it was transferred to a round bottom flask and stirred at 90 ^{o}C in an oil bath for 5.0 h. After cooling to room temperature, the resulting stable black dispersion was centrifuged at 16000 rpm and washed with DW for three times. Finally, the RGO material was obtained by freeze-drying.

2.5 Preparation of the Pd@RGO

For preparation of the Pd@RGO material, 10.0 mg RGO was dispersed into 20.0 mL of DW via sonication. Then 0.80 mL of 5.0 mM $PdCl_2$ aqueous solution was added to the RGO suspension dropwise and stirred in an ice bath for 0.5 h. After centrifuging and washing with DW for three times, the resulting Pd@RGO was obtained by freeze-drying.

2.6 Synthesis of SS-β-CD dimer

SS-β-CD dimer was synthesized using the method reported by Tang and co-workers. [52] Briefly, the SH-β-CD (2.0 g) was dissolved in 10% H_2O_2 (25 mL) by heating, and the mixture was stirred at room temperature for 5 h. A white precipitate was obtained after the solvent was added to acetone. The precipitate was filtered. After evaporation of acetone and water in vacuo, SS-β-CD dimer was obtained. The yield of the SS-β-CD was calculated to be 94.1%.

2.7 Preparation of the SS-β-CD-Pd@RGO nanohybrids

The fabrication of the SS-β-CD-Pd@RGO nanohybrid was carried out by sonicating 10 mg of Pd@RGO in 20 mL of 0.5 mg mL^{-1} SS-β-CD at room temperature for 2 h and stirred for another 10 h. Finally, the resulting stable black suspension was centrifuged and washed with DW for three times to remove unbound SS-β-CD, and then lyophilized to obtain SS-β-CD-Pd@RGO nanohybrid. The β-CD-Pd@RGO composite was prepared using the similar procedure by replacing SS-β-CD with native β-CD.

2.8 Preparation of the modified electrodes

GC electrode (3 mm in diameter) was polished with 0.3 and 0.05 μm Al_2O_3 powder respectively and subsequently sonicated in ethanol and DW to remove the adsorbed substance and dried in air. The SS-β-CD-Pd@RGO was dispersed in DW at a concentration of 0.5 mg mL^{-1} with the aid of ultrasonic agitation for 20 min, resulting in a homogeneous suspension. To prepare the SS-β-CD-Pd@RGO modified electrode, 5 μL of the SS-β-CD-Pd@RGO suspension was dropped onto the electrode surface and dried at room temperature. The obtained electrode was noted as SS-β-CD-Pd@RGO/GC electrode. The β-CD-Pd@RGO/GC, Pd@RGO/GC, and RGO/GC electrodes were prepared in the same way.

2.9 Electrochemical measurements

Before electrochemical measurements, the RGO/GC, Pd@RGO/GC, β-CD-Pd@RGO/GC, and SS-β-CD-Pd@RGO/GC electrodes were electrochemically

reduced in 0.1 M phosphate buffer (PBS, pH 7.0) by cycling the potential between 0 and −1.4 V for 15 cycles. Prior to the electrochemical reduction, the PBS was completely saturated with nitrogen gas to remove the dissolved oxygen. After that, DPV was carried out 0.1 M PBS (pH 3.0) containing different concentrations of baicalin and luteolin by scanning the potential from 0.0 to 0.7 V with an amplitude of 0.05 V and a pulse width of 0.05 s. EIS was recorded in the frequency range from 10^1 to 10^5 Hz with an amplitude of 5 mV using 2.0 mM $[Fe(CN)_6]^{3-/4-}$ redox couple (1:1) with 0.1 M KCl as supporting electrolyte. All the measurements were carried out at room temperature.

3. Results and Discussion

3.1 UV-vis spectroscopic measurements

The UV-vis spectroscopy was used to investigate the interactions between baicalin and SS-β-CD or β-CD. As shown in **Fig. 1A**, the baicalin shows two strong absorptions at 277 and 318 nm, respectively. The two absorbances increased slightly when the β-CD was added to the aqueous solution of baicalin. However, significant increases of the two absorbances were observed when the SS-β-CD was added to the aqueous solution of baicalin. Complexation of baicalin with SS-β-CD exhibited greatly enhanced absorbances compared to the complexation with native β-CD. The luteolin shows two strong absorptions at 269 and 352 nm, respectively, as shown in **Fig. 1B**. Similar to baicalin, complexation of luteolin with SS-β-CD exhibited greatly enhanced absorbances compared to the complexation with native β-CD. The enhanced

243 absorbances was caused by the cooperative binding of two adjacent hydrophobic
244 cavities with baicalin in SS-β-CD. [41,43,53]
245
246 **3.2 Characterization of the SS-β-CD-Pd@/RGO nanohybrids**
247 The SEM image of RGO was obtained as shown in **Fig. S1**. The microstructure
248 image reveals that the RGO material consists of randomly aggregated thin, wrinkled
249 sheets closely associated with each other. The morphologies and microstructures of
250 Pd@RGO was investigated by TEM observation as shown in **Figs. 2A–C**. The most
251 striking feature is that the Pd clusters with a uniform size ~2.0 nm are fairly well
252 monodispersed on the surface of RGO. The driving force for Pd clusters deposition on
253 RGO could be caused by the redox reaction between Pd^{2+} and RGO. The RGO is the
254 electron donors or the reductants for subsequent Pd cluster growth on the RGO
255 surface. Previous reports have explored that both single-wall carbon nanotubes
256 (SWNTs) [54] and GO [25] could, respectively, reduce $AuCl_4^{3-}$ and $PdCl_4^{2-}$ to generate Au
257 NPs and Pd NPs without any additional reductant. These phenomena are explained by
258 the difference in the redox potentials of $AuCl_4^{3-}$ ions and SWNTs (0.5 V *vs* SCE) or
259 $PdCl_4^{2-}$ and GO (0.48 V *vs* SCE), which facilitates the reduction of noble metal ions.
260 Similar to these carbon materials, RGO is also good reducing agents for the formation
261 of Pd@RGO nanocomposites. The small size of Pd clusters deposited on the RGO
262 surface indicates that the remaining oxygen-containing groups, (generally the
263 graphene produced via the reduction method has some oxygen-containing groups),
264 may play an important role in controlling the formation of Pd clusters through

increasing the anchoring ability of Pd nuclei on the RGO surface and avoiding Ostwald ripening following nuclei. [25] The β-CD-Pd@RGO and SS-β-CD-Pd@RGO nanohybrids were characterized by FTIR and TGA analysis. **Fig. 2D** shows the FTIR spectra of the RGO, β-CD-Pd@RGO, and SS-β-CD-Pd@RGO materials. It is found that the FTIR spectrum of RGO is essentially featureless except some weak absorptions of the remaining oxygen-containing groups. Whereas the FTIR spectra of β-CD-Pd@RGO and SS-β-CD-Pd@RGO exhibit the typical CD absorption features of the coupled C–O–C stretching/O–H bending vibrations at 1204 cm^{-1}, the coupled C–O/C–C stretching/O–H bending vibrations at 1090 cm^{-1}, and O–H stretching vibrations at 3435 cm^{-1}. The presence of these peaks confirmed that the β-CD and SS-β-CD molecules were successfully attached to the surface of the Gra. The prepared SS-β-CD-Pd@RGO and the related materials were also characterized by TGA, as shown in **Fig. 2E**. For the pristine RGO, there is a minor loss in mass (24%) at a temperature of approximately 600 °C owing to the pyrolysis of a small amount of the labile oxygen-containing functional groups. The β-CD-Pd@RGO material exhibited an abrupt mass loss when the temperature was approximately 260 ^{o}C because of the decomposition of β-CD; the mass loss reached about 60 wt% when the temperature was 600 ^{o}C. Similarly, the SS-β-CD-Pd@RGO nanohybrid also exhibited an abrupt mass loss when the temperature was approximately 260 ^{o}C owing to the decomposition of SS-β-CD; the mass loss reached approximately 61 wt% when the temperature was 600 ^{o}C. The amount of β-CD and SS-β-CD grafted to RGO were estimated to be approximately 36.0% and 37.0%, respectively. It should be noted here

that the amount of SS-β-CD attached to RGO is approximately equal to that of β-CD.

3.3 Electrochemical characterization of the modified electrodes

The value of the charge transfer resistance (R_{ct}) of the modified electrode was estimated by the semicircle diameter. **Fig. 2F** illustrates the EIS of the bare GCE, RGO/GCE, Pd@RGO/GCE, β-CD-Pd@RGO/GCE, and SS-β-CD-Pd@RGO/GCE. Obviously, the bare GCE exhibited a semicircle portion and the value of R_{ct} was estimated to be approximately 800 Ω. While the R_{ct} decreased dramatically, nearly to zero at RGO/GCE, indicating that RGO/GCE formed high electron conduction pathways between the electrode and electrolyte. When the Pd@RGO modified on the bare GCE, the semicircle decreased further, revealing that Pd clusters with excellent conductivity can facilitate the electron transfer. For the β-CD-Pd@RGO/GCE and SS-β-CD-Pd@RGO/GCE, their semicircles both increased to approximately 1500 Ω. This is because of the β-CD or SS-β-CD layer hindered the electron transfer and made the interfacial charge transfer difficult. The β-CD and SS-β-CD are successfully immobilized of on the graphene, which was directly proved by the TGA analysis. The increased R_{ct} is not a direct proof that β-CD or SS-β-CD are immobilized on the grapheme. but it can be a auxiliary evidence.

The kinetics of the electrode reactions was investigated by studying the effect of scan rate at the SS-β-CD-Pd@RGO/GCE using 2.0 mM $[Fe(CN)_6]^{3-/4-}$ redox couple (1:1) with 0.1 M KCl as supporting electrolyte. As shown in **Fig. S2A**, both anodic peak current (I_{pa}) and cathodic peak current (I_{pc}) increased with the increase of scan

rate in the range of 50–400 mV s^{-1}. Also, the I_{pa} and I_{pc} showed a linear relationship with the scan rate respectively (**Fig. S2B**), suggesting that the electrode reaction is a adsorption-controlled electrochemical process. [55] It can be seen that both I_{pa} and I_{pc} of the modified electrode increased linearly and were proportional to the scan rate according to Eqs. I_{pa} (μA) = 0.30 v (mV/s) + 36.3 and I_{pc} (μA) = −0.27 v (mV/s) – 65.3. The separation of peaks suggests that the process is not perfectly reversible; however, stable redox peak current and position during repeated scans at a particular scan rate suggests that the SS-β-CD-Pd@RGO/GCE exhibit a quasi-reversible process. [56] Moreover, both anodic peak potential (E_{pa}) and cathodic peak potential (E_{pc}) demonstrated a linear relationship with the scan rate respectively (**Fig. S2C**), indicating that the electron transport form redox moieties to the electrode is very facile. [57]

3.4 Electrochemical behavior of baicalin and luteolin on the modified electrodes

The electrochemical behaviors of baicalin and luteolin toward the modified electrodes were investigated using CV and DPV. The CVs for the oxidation and reduction of 20 μM baicalin at bare GCE, RGO/GCE, Pd@RGO/GCE, β-CD–Pd@RGO/GCE, and SS-β-CD–Pd@RGO/GCE were obtained in 0.1 M PBS (pH 3.0) as shown in **Fig. 3A**. Enhanced redox currents of baicalin using the RGO-modified GCE were observed in comparison with that in the bare GCE. This increase indicated that the high surface area and high conductivity of the RGO increased the effective electrode area and improved the electroactivity towards

baicalin oxidation and reduction. Another reason for the enhancement of the currents at the RGO-modified GCE is considered to be the π–π interaction between the baicalin and the RGO film on the GCE. [58] In the case of Pd@RGO/GCE, the redox currents of baicalin were enhanced compared with that of the RGO-modified GCE, indicating that Pd clusters with excellent conductivity can amplify the electrochemical signal. Generally, an increase in the peak current and a decrease in the peak potential could be ascribed to the electrocatalysis. However, the peak potential here is almost no change. Recently, Compton et al. reported that the electrochemical reaction at a thin film-modified electrode being facilitated without a change in the electrochemical rate constant could be considered to alter the solubilities and diffusion coefficients of the electroactive species. [59] Thus, the enhancement of the redox currents at Pd@RGO/GCE may also be caused by the altered solubilities or diffusion coefficients of the electroactive species. In addition, the redox currents increased remarkably when the β-CD–Pd@RGO nanohybrid was immobilized onto the surface of GCE. This may be attributed to the β-CD molecules with excellent supramolecular recognition capability that formed inclusion complexes with baicalin. Interestingly, due to the cooperative binding abilities of two adjacent CD units, the redox currents of baicalin at SS-β-CD–Pd@RGO/GCE increased dramatically. This result demonstrated that SS-β-CD possesses higher supramolecular recognition capability than the native β-CD. The CVs for the oxidation and reduction of 10 μM luteolin at bare GCE, RGO/GCE, Pd@RGO/GCE, β-CD–Pd@RGO/GCE, and SS-β-CD–Pd@RGO/GCE in 0.1 M PBS (pH 3.0) were also obtained as shown in **Fig.**

3B. Similar to baicalin, the redox currents of luteolin at the modified electrodes increased in sequence. As can been seen, the peak to peak potential difference both for baicalin and luteolin in **Fig. 3A and B** that were close to 0 mV, indicated that the process was adsorption controlled. [55]

Fig. S3A shows the CVs of 20 μM baicalin at SS-β-CD–Pd@RGO/GCE for different scan rates. The accumulation condition was carried out at −0.2 V for 200 s. Both anodic peak current (I_{pa}) and cathodic peak current (I_{pc}) increase gradually with an increase in scan rate. As shown in **Fig. S3B**, the peak current increases linearly with the scan rate in the 50 to 400 mV s^{-1} range, and the equation can be expressed as I_{pa} (μA) = 0.136 v (mV/s) + 9.15 (R^2 = 0.9985) and I_{pc} (μA) = −0.042 v (mV/s) + 0.757. The representation of redox peak current vs. scan rate was linear, indicating that in this case, the process was adsorption controlled. [55] In addition, both anodic peak potential (E_{pa}) and cathodic peak potential (E_{pc}) demonstrated a linear relationship with the scan rate respectively (**Fig. S3C**).

Similarly, the effect of scan rate on the redox of luteolin was also studied. **Fig. S4A** shows the CVs of 10 μM luteolin at SS-β-CD–Pd@RGO/GCE for different scan rates. As shown in **Fig. S4B**, both anodic peak current (I_{pa}) and cathodic peak current (I_{pc}) increase linearly with the scan rate in the 50 to 400 mV s^{-1} range, and the equation can be expressed as I_{pa} (μA) = 0.155 v (mV/s) + 10.59 (R^2 = 0.9985) and I_{pc} (μA) = −0.146 v (mV/s) − 7.05, indicating that the redox of luteolin on SS-β-CD–Pd@RGO/GCE is a typical adsorption-controlled process. [55] Also, both anodic peak potential (E_{pa}) and cathodic peak potential (E_{pc}) demonstrated a linear

relationship with the scan rate respectively (**Fig. S4C**).

The DPVs for the oxidation of 20 μM baicalin at bare GCE, RGO/GCE, Pd@RGO/GCE, β-CD–Pd@RGO/GCE, and SS-β-CD–Pd@RGO/GCE were obtained in 0.1 M PBS (pH 3.0) as shown in **Fig. 3C**. The oxidation of 20 μM baicalin at the bare GCE showed a small peak current of 1.5 μA. Enhanced oxidation peak current of baicalin using the RGO-modified GCE was observed in comparison with that in the bare GCE. In the case of Pd@RGO/GCE, the oxidation current of baicalin was enhanced compared with that of the RGO-modified GCE. In addition, the oxidation current increased remarkably when the β-CD–Pd@RGO nanohybrid was immobilized onto the surface of GCE. Furthermore, the oxidation current of baicalin at SS-β-CD–Pd@RGO/GCE increased dramatically, which is 1.5 and 24.8 times higher than that of the β-CD–Pd@RGO/GC and bare GC electrodes, respectively. The DPV results were in accordance with that of CV. Although the amount of SS-β-CD attached to RGO measured by TGA is approximately equal to that of β-CD, the higher oxidation peak current of baicalin at SS-β-CD–Pd@RGO/GCE than that at β-CD–Pd@RGO/GCE was obtained. This is only caused by the higher supramolecular recognition capability of SS-β-CD. The DPVs for the oxidation of 10 μM luteolin at bare GCE, RGO/GCE, Pd@RGO/GCE, β-CD–Pd@RGO/GCE, and SS-β-CD–Pd@RGO/GCE in 0.1 M PBS (pH 3.0) were also obtained as shown in **Fig. 3D**. Similar to baicalin, the oxidation peak currents of luteolin at the modified electrodes increased in sequence, indicating that the SS-β-CD–Pd@RGO/GCE nanohybrid is highly suitable for the detection of baicalin

and luteolin by combining the merits of Pd@RGO and SS-β-CD. **Fig. 3E** shows the oxidation of 20 μM of baicalin (a), 10 μM of luteolin (b), and a mixture (c) containing 20 μM of baicalin and 10 μM of luteolin at the SS-β-CD–Pd@RGO/GCE in 0.1 M PBS (pH 3.0). Two well-defined peaks that were present at 0.30 and 0.42 V corresponded to baicalin and luteolin, respectively, which were well separated from each other with a potential difference of 120 mV. The potential differences were large enough to simultaneously determine the concentrations of baicalin and luteolin. **Fig. 3F** shows the oxidation of a mixture containing 20 μM of baicalin and 10 μM of luteolin at bare GCE, RGO/GCE, Pd@RGO/GCE, β-CD–Pd@RGO/GCE, and SS-β-CD–Pd@RGO/GCE in 0.1 M pH 3.0 PBS. Improved oxidation currents of baicalin and luteolin using these modified electrode were observed. The results are in accordance with that for individual baicalin and luteolin in **Figs. 3C and D**. These results suggested that the SS-β-CD–Pd@RGO nanohybrid-modified electrode was a better electrode for the simultaneous electrochemical sensing of baicalin and luteolin than β-CD–Pd@RGO/GCE.

3.5 Simultaneous determination of baicalin and luteolin using DPV

Under optimal conditions (the optimal solution pH is 3.0, the optimal accumulation condition is −0.2 V for 200 s, see **ESI** for details), DPV was used to determine the concentrations of baicalin and luteolin because it is a highly sensitive and low-detection limit electrochemical method. **Fig. 4A** shows the DPV curves of baicalin and luteolin on the SS-β-CD–Pd@RGO/GCE under the different solution

concentrations. The oxidation peak currents increased with the increased baicalin and luteolin concentrations. **Fig. 4B** shows the corresponding calibration curve for baicalin. The oxidation currents were proportional to the baicalin concentrations between 0.02 and 20.0 μM with a detection limit of 0.0052 μM (*S/N = 3*). The corresponding regression equation was calculated as I (μA) = 1.88C (μM) + 1.12 with a correlation coefficient of 0.996. **Fig. 4C** shows the corresponding calibration curve for luteolin. The oxidation currents were also proportional to the concentration of luteolin between 0.01 and 10.0 μM with a detection limit of 0.0070 μM (*S/N = 3*). The corresponding regression equation was calculated as I (μA) = 3.80C (μM) + 1.27 with a correlation coefficient of 0.995. The performance of the proposed SS-β-CD–Pd@RGO-modified electrode was compared with those of other reported electrodes. **Table 1** shows that the SS-β-CD–Pd@RGO/GCE exhibited a lower detection limit and wider linear range than the other electrodes. Thus, the modified electrode that was fabricated can be used to simultaneously detect baicalin and luteolin in solutions with high sensitivity. In the present work, the excellent detection performance of the proposed electrochemical sensor may be attributed to two factors: (1) the RGO with the unique structure and outstanding properties (good electrochemical properties and large surface area) loaded lots of Pd clusters and large amount of SS-β-CD; (2) the SS-β-CD with higher supramolecular recognition and enrichment capability than the native β-CD provided more binding sites for recognition abundant of guest molecules.

3.6 Selectivity, reproducibility, and stability

Interference during the simultaneous detection of baicalin and luteolin was caused by glucose, oxalic acid, citric acid, urea, ascorbic acid, uric acid, dopamine, which were studied using the SS-β-CD–Pd@RGO-modified GCE. The currents for oxidation of 20 μM of baicalin and 10 μM of luteolin at the SS-β-CD–Pd@RGO/GC electrode were compared with the signal obtained in the presence of interfering species. As shown in **Fig. S10**, a ten-fold concentration of glucose, oxalic acid, citric acid, urea, and AA did not affect the baicalin and luteolin responses. In addition, no significant interference from common ions, such as Na^{+}, K^{+}, Ca^{2+}, Mg^{2+}, Cl^{-}, NO_3^{-}, SO_4^{2-}, CO_3^{2-}, Cu^{2+}, Zn^{2+}, and Al^{3+}, was observed, even at 100-fold excess concentrations (Data not shown). Thus, the simultaneous and quantitative detection of baicalin and luteolin was reliable at ambient conditions.

The oxidation peak currents of 20 μM of baicalin and 10 μM of luteolin using six equal SS-β-CD–Pd@RGO/GCEs were compared to evaluate the fabrication reproducibility of the SS-β-CD–Pd@RGO-modified electrode. The six modified electrodes exhibited similar electrochemical responses with a relative standard deviation (RSD) of 4.6%, indicating satisfactory reproducibility.

Successive cyclic potential scans for 50 cycles and long-term storage assays were used to examine the stability of the SS-β-CD–Pd@RGO-modified electrode. A 7.5% decrease in the initial peak current was observed after 30 continuous cycle scans. Additionally, a long-term stability experiment was performed intermittently (every 5 days). The constructed sensor was stored in a refrigerator at 4 °C when not in use.

463 Initial responses of over 94.2% and 84.6% remained after storage for 15 and 30 days,
464 respectively, revealing an acceptable stability of the SS-β-CD–Pd@RGO-modified
465 electrode.
466
467 **3.7 Real sample analysis and potential application of the constructed sensor**
468 The SS-β-CD–Pd@RGO/GCE sensor was used to detect baicalin and luteolin in
469 human serum samples using standard addition methods to evaluate the feasibility of
470 the SS-β-CD–Pd@RGO-modified electrode for real sample analysis. The serum
471 sample was diluted one hundred times with 0.1 M PBS (pH 3.0). Results showed
472 apparent recoveries ranging from 96.6% to 106.0% and RSDs ranging from 2.9% to
473 5.6% (**Table 2**). These findings demonstrated that the SS-β-CD–Pd@RGO-based
474 sensor that was fabricated in this study has practical applications.
475 The proposed sensor may also be expanded to potential applications in biological
476 and functional food samples. It is worth noting that, as an oligosaccharide, SS-β-CD
477 is stable enough under complex conditions, and thus seems to be more suitable for
478 analysis of practical samples. In addition, SS-β-CD possesses higher molecular
479 recognition capability than native β-CD and its synthesis is very easy. Therefore, this
480 sensor could be used to determine the flavonoids in biological samples and provide
481 new opportunities for analysis of flavonoids metabolites in organisms in the future.
482
483 **4. Conclusions**
484 In summary, by combining the merits of Pd@RGO and the SS-β-CD, a highly

485 sensitive electrochemical sensing platform was developed based on the
486 SS-β-CD-Pd@RGO nanohybrids. Electrochemical simultaneous detection of baicalin
487 and luteolin using SS-β-CD-Pd@RGO nanohybrids-modified electrode is described
488 for the first time. Due to the synergistic effects from the Pd@RGO and SS-β-CD, the
489 SS-β-CD-Pd@RGO modified GC electrode was found to have linear response ranges
490 of 0.02–20.00 μM for baicalin and 0.01–10.00 μM for luteolin with relatively low
491 detection limits of 0.0052 μM for baicalin and 0.0070 μM for luteolin, respectively,
492 implying that SS-β-CD-Pd@RGO nanohybrids are excellent sensing materials for the
493 electrochemical determination of flavonoids. In addition, the proposed sensing
494 platform was employed for detection of baicalin and luteolin in human serum samples
495 with satisfactory results. Thus, the present work might broaden the electrochemical
496 application of various bridged bis(β-CD)s in electrochemical sensing or biosensing
497 field.
498
499 **Acknowledgements**
500 This work was supported by the Natural Science Foundation of China (31160334)
501 and the Natural Science Foundation of Yunnan Province (2012FB112, 2014RA022),
502 People's Republic of China.
503
504 **References:**
505 1 L. Zhang, A. S. Ravipati, S. R. Koyyalamudi, S. C. Jeong, N. Reddy, P. T. Smith,
506 J. Bartlett, K. Shanmugam, G. Münch, M. J. Wu, *J. Agric. Food Chem.*, 2011, **59**,

12361–12367.

2 M. E. Carlotti, S. Sapino, E. Ugazio, G. Caron, *J. Incl. Phenom. Macro.*, 2010, **70**, 81–90.

3 E. Pinho, M. Grootveld, G. Soares, M. Henriques, *Carbohyd. Polym.*, 2014, **101**, 121–135.

4 D. D. Orhan, B. Ozçelik, S. Ozgen, F. Ergun, *Microbiol. Res.*, 2010, **165**, 496–504.

5 M. Okamoto, M. Ohta, H. Kakomn, T. Omori, *Chromatographia*, 1993, **35**, 281–284.

6 S. J. Sheu, C. F. Lu, *J. High Resolut. Chromatogr.*, 1996, **19**, 409–412.

7 Y. M. Liu, S. J. Sheu, *Anal. Chim. Acta*, 1994, **288**, 221–226.

8 C. S. Liu, Y. S. Song, K. J. Zhang, J. C. Ryu, M. Kim, T. H. Zhou, *J. Pharm. Biomed. Anal.*, 1995, **13**, 1409–1414.

9 M. C. Lin, M. J. Tsai, K. C. Wen, *J. Chromatogr. A*, 1999, **830**, 387–395.

10 Q. Chang, M. Zhu, Z. Zuo, M. Chow, W. K. Ho, *J. Chromatogr. B: Biomed. Sci. Appl.*, 2001, **760**, 227–235.

11 F. M. Areias, P. Valentao, P. B. Andrade, F. Ferreres, R. M. Seabra, *Food Chem.*, 2001, **73**, 307–311.

12 S. M. Wittemer, M. Veit, *J. Chromatogr. B*, 2003, **793**, 367–375.

13 G. Favaro, C. Clementi, A. Romani, V. Vickackaite, *J. Fluoresc.*, 2007, **17**, 707–714.

14 J. G. Renee, C. K. Geoffrey, A. Z. Mamdouh, J. A. Louise, *Phytochem. Anal.*,

2000, **11**, 257–267.

15 D. A. van Elswijk, U. P. Schobel, E. P. Lansky, H. Irth, J. van der Greef, *Phytochemistry*, 2004, **65**, 233–241.

16 D. M. Zhao, X. H. Zhang, L. J. Feng, Q. Qi, S. F. Wang, *Food Chem.*, 2011, **127**, 694–698.

17 S. H. Wu, B. J. Zhu, Z. X. Huang, J.. J. Sun, *Electrochem. Commun.*, 2013, **28**, 47–50.

18 Z. Liu, A. Zhang, Y. Guo, C. Dong, *Biosens. Bioelectron.*, 2014, **58**, 242-248.

19 P. F. Pang, Y. P. Liu, Y. L. Zhang, Y. T. Gao, Q. F. Hu, *Sens. Actuators B*, 2014, **194**, 397–403.

20 A. Y. Tesio, A. M. Granero, N. R. Vettorazzi, N. F. Ferreyra, G. A. Rivas, H. Fernández, M. A. Zon, *Microchem. J.*, 2014, **115**, 100–105.

21 H. Ibrahim, Y. Temerk, *Sens. Actuators B*, 2015, **206**, 744–752.

22 M. L. Pang, J. Y. Hu, H. C. Zeng, *J. Am. Chem. Soc.*, 2010, **132**, 10771–10785.

23 J. A. Farmer, C. T. Campbell, *Science*, 2010, **329**, 933–936.

24 R. J. White, R. Luque, V. L. Budarin, J. H. Clark, D. J. Macquarrie, *Chem. Soc. Rev.*, 2009, **38**, 481–494.

25 X. M. Chen, G. H. Wu, J. M. Chen, X. Chen, Z. X. Xie, X. R. Wang, *J. Am. Chem. Soc.*, 2011, **133**, 3693–3695.

26 W. Chen, S. Chen, *Angew. Chem., Int. Ed.*, 2009, **48**, 4386–4389.

27 H. J. Yin, H. J. Tang, D. Wang, Y. Gao, Z. Y. Tang, *ACS Nano*, 2012, **6**, 8288–8297.

28 Y. J. Wang, D. P. Wilkinson, J. Zhang, *Chem. Rev.*, 2011, **111**, 7625–7651.

29 M. J. Allen, V. C. Tung, R. B. Kaner, *Chem. Rev.*, 2010, **110**, 132–145.

30 L. Yang, H. Zhao, S. Fan, B. Li, C.-P. Li, *Anal. Chim. Acta*, 2014, **852**, 28-36.

31 J. Zhou, M. Chen, G. W. Diao, *ACS Appl. Mater. Interfaces*, 2013, **5**, 828−836.

32 G. Zheng, M. Chen, X. Y. Liu, J. Zhou, J. Xie, G. W. Diao, *Electrochim. Acta*, 2014, **136**, 301–309.

33 M. Chen, Y. Meng, W. Zhang, J. Zhou, J. Xie, G. W. Diao, *Electrochim. Acta*, 2013, **108**, 1– 9.

34 Y. Yao, L. Zhang, J. Xu, X. Wang, X. Duan, Y. Wen, *J. Electroanal. Chem.*, 2014, **713**, 1–8.

35 J. M. Gong, X. M. Han, X. L. Zhu, Z. Q. Guan, *Biosens. Bioelectron.*, 2014, **61**, 379–385.

36 L. Yang, H. Zhao, Y. C. Li, C.-P. Li, *Sens. Actuators B*, 2015, **207**, 1–8.

37 L. Yang, S. Fan, G. Deng, Y. Li, X. Ran, H. Zhao, C.-P. Li, *Biosens. Bioelectron.*, 2015, **68**, 617–625.

38 L. Yang, H. Zhao, C.-P. Li, S. M. Fan, B. C. Li, *Biosens. Bioelectron.*, 2015, **64**, 126–130.

39 Y. Guo, S. Guo, J. Ren, Y. Zhai, S. Dong, E. Wang, *ACS Nano*, 2010, **4**, 4001–4010.

40 G. Zhu, X. Zhang, P. Gai, X. Zhang, J. Chen, *Nanoscale*, 2012, **4**, 5703–5709.

41 Y. Zhao, J. Gu, Y. C. Yang, H. Y. Zhu, R. Huang, B. Jing, *J. Mol. Struct.*, 2009, **930**, 72–77.

42 P. Li, Y. Liu, X. Wang, B. Tang, *Analyst*, 2011, **136**, 4520–4525.

43 Y.-M. Zhang, H.-Z. Chen, Y. Chen, F. Ding, Y. Liu, *New J. Chem.*, 2013, **37**, 1554–1560.

44 Y. Liu, B. Li, C. C. You, T. Wada, Y. Inoue, *J. Org. Chem.*, 2001, **66**, 225–232.

45 Y. Okabe, H. Yamamura, K. Obe, K. Ohta, M. Kawai, K. Fujita, *Chem. Commun.*, 1995, **5**, 581–582.

46 T. Jiang, D. K. Sukumaran, S. D. Soni, D. S. Lawrence, *J. Org. Chem.*, 1994, **59**, 5149–5155.

47 H. F. M. Nelissen, M. Feiters, R. J. M. Nolte, *J. Org. Chem.*, 2002, **67**, 5901–5906.

48 Y. Hasegawa, M. Miyauchi, Y. Takashima, H. Yamaguchi, A. Harada, *Macromolecules*, 2005, **38**, 3724–3730.

49 Y. Liu,; Y. W. Yang,; Y. Zhao,; L. Li,; H. Y. Zhang,; S. Z. Kang, *J. Inclusion Phenom. Macrocyclic Chem.*, 2003, **47**, 155–160.

50 T. Ogoshi, M. Hashizume, T. Yamagishi, Y. Nakamoto, *Langmuir*, 2010, **26**, 3169–3173.

51 X. B. Fan, W. C. Peng, Y. Li, X. Y. Li, S. L. Wang, G. L. Zhang, F. B. Zhang, *Adv. Mater.*, 2008, **20**, 4490–4493.

52 B. Tang, H. Liang, K. Xu, Z. Mao, X. Shi, Z. Chen, *Anal. Chim. Ac*ta, 2005, **554**, 31–36.

53 D. Chen, Z. Chen, K. Xu, B. Tang, *J. Agric. Food Chem.*, 2011, **59**, 4424–4428.

54 H. C. Choi, M. Shim, S. Bangsaruntip, H. Dai, *J. Am. Chem. Soc.*, 2002, **124**,

9058–9059.

55 J. Molina, J. Fernández, C. García, A. I. del Río, J. Bonastre, F. Cases, *Electrochim., Acta*, 2015, **166**, 54–63.

56 E. Topoglidis, Y. Astuti, F. Duriaux, M. Gratzel, J. R. Durrant, *Langmuir*, 2003, **19**, 6894–6900.

57 A. Kaushik, A. Vasudev, S. K. Arya, , S. Bhansali, *Biosens. Bioelectron.*, 2013, **50**, 35–41.

58 M. A. Raj, S. A. J ohn, *Anal. Chim. Acta*, 2013, **771**, 14–20.

59 W. G. Hepburn, C. Batchelor-McAuley, K. Tschulik, E. O. Barnes, R. T. Kachoosangi, R. G. Compton, *Phys. Chem. Chem. Phys.*, 2014, **16**, 18034–18041.

60 G. Chen, H. Zhang, J. Ye, *Talanta*, 2000, **53**, 471–479.

61 D. Lu, S. Lin, L. Wang, T. Li, C. Wang, Y. Zhang, *J. Solid State Electrochem.*, 2014, **18**, 269–278.

Figure captions:

Scheme 1. Chemical structures of baicalin **(A)** and luteolin **(B)**.

Scheme 2. The illustration of the SS-β-CD-Pd@RGO nanohybrids simultaneously sensing baicalin and luteolin by an electrochemical strategy.

Fig. 1. (A) UV-vis spectra of free baicalin (50 μM), 50 μM baicalin + 0.72 mM β-CD,

50 μM baicalin + 0.32 mM SS-β-CD, free β-CD (0.72 mM), and free SS-β-CD (0.32 mM) in aqueous solution. **(B)** UV-vis spectra of free luteolin (50 μM), 50 μM luteolin + 0.72 mM β-CD, 50 μM luteolin + 0.32 mM SS-β-CD, free β-CD (0.72 mM), and free SS-β-CD (0.32 mM) in aqueous solution.

Fig. 2. (A–C) TEM images of Pd@RGO at different magnifications. **(D)** FTIR spectra of RGO, β-CD-Pd@RGO, and SS-β-CD-Pd@RGO. **(E)** TGA curves of RGO, β-CD-Pd@RGO, and SS-β-CD-Pd@RGO. **(F)** EIS characterization of bare GCE, RGO/GCE, Pd@RGO/GCE, β-CD-Pd@RGO/GCE, and SS-β-CD-Pd@RGO/GCE using 2.0 mM $[Fe(CN)_6]^{3-/4-}$ redox couple (1:1) with 0.1 M KCl as supporting electrolyte.

Fig. 3. CVs of 20 μM baicalin **(A)** and 10 μM luteolin **(B)** at bare GCE, RGO/GCE, Pd@RGO/GCE, β-CD-Pd@RGO/GCE, and SS-β-CD-Pd@RGO/GCE in 0.1 M PBS (pH 3.0). DPVs of 20 μM baicalin **(C)** and 10 μM luteolin **(D)** at bare GCE, RGO/GCE, Pd@RGO/GCE, β-CD-Pd@RGO/GCE, and SS-β-CD-Pd@RGO/GCE in 0.1 M PBS (pH 3.0). **(E)** DPVs obtained for the oxidation of 20 μM baicalin (a), 10 μM of luteolin (b), and a mixture (c) containing 20 μM baicalin and 10 μM of luteolin at the SS-β-CD-Pd@RGO/GCE in 0.1 M PBS (pH 3.0). **(F)** DPVs obtained for the oxidation of a mixture containing 20 μM of baicalin and 10 μM of luteolin at bare GCE, RGO/GCE, Pd@RGO/GCE, β-CD-Pd@RGO/GCE, and SS-β-CD-Pd@RGO/GCE in 0.1 M PBS (pH 3.0). Pulse width: 0.05 s; amplitude:

0.05 V.

Fig. 4. (A) DPV curves obtained for the oxidation of baicalin and luteolin at SS-β-CD-Pd@RGO/GCE for different concentrations. Calibration curves for simultaneous determination of baicalin **(B)** and luteolin **(C)** using the proposed sensor. The error bars represent the standard deviations of three parallel tests.

Figures:

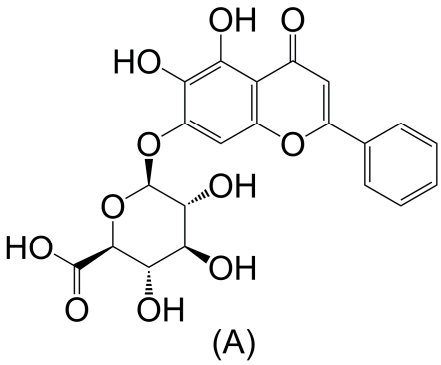

(A)

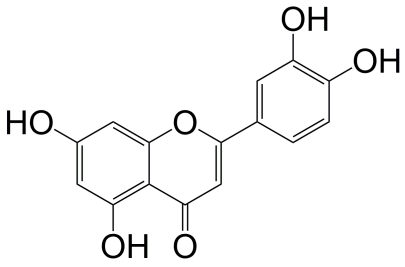

(B)

Scheme 1

Ran et al.

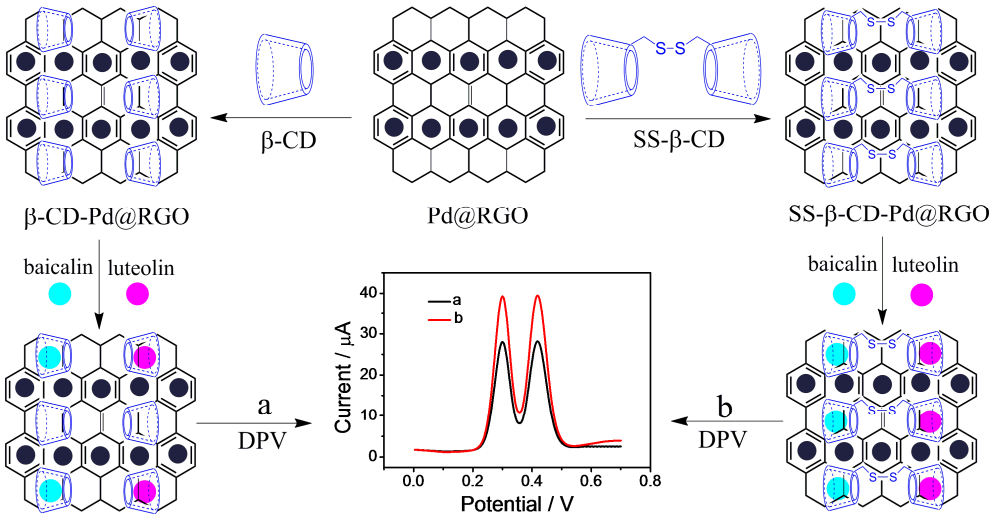

Scheme 2

Ran et al.

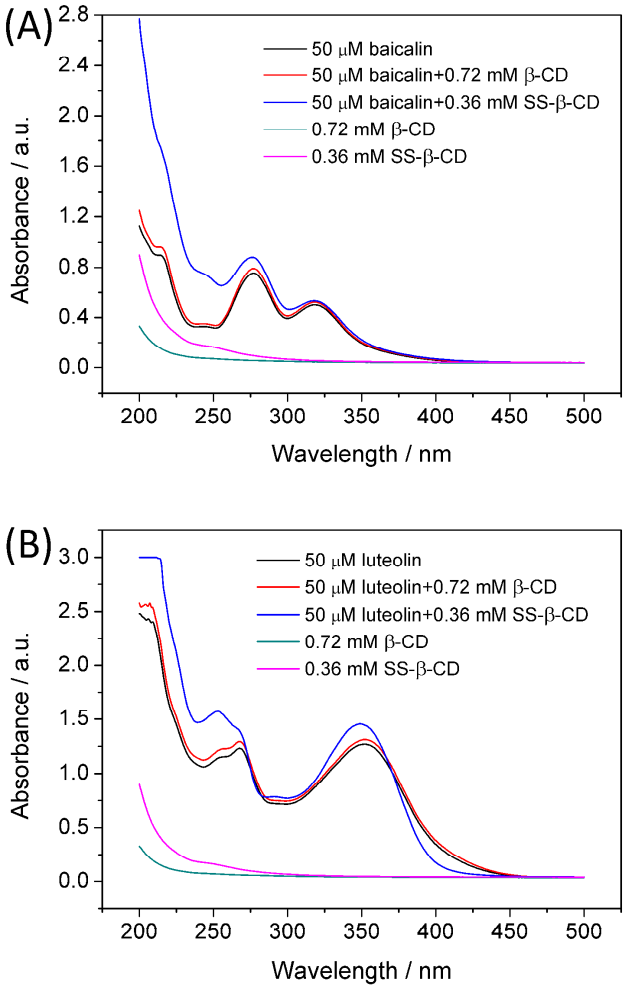

Fig. 1

Ran et al.

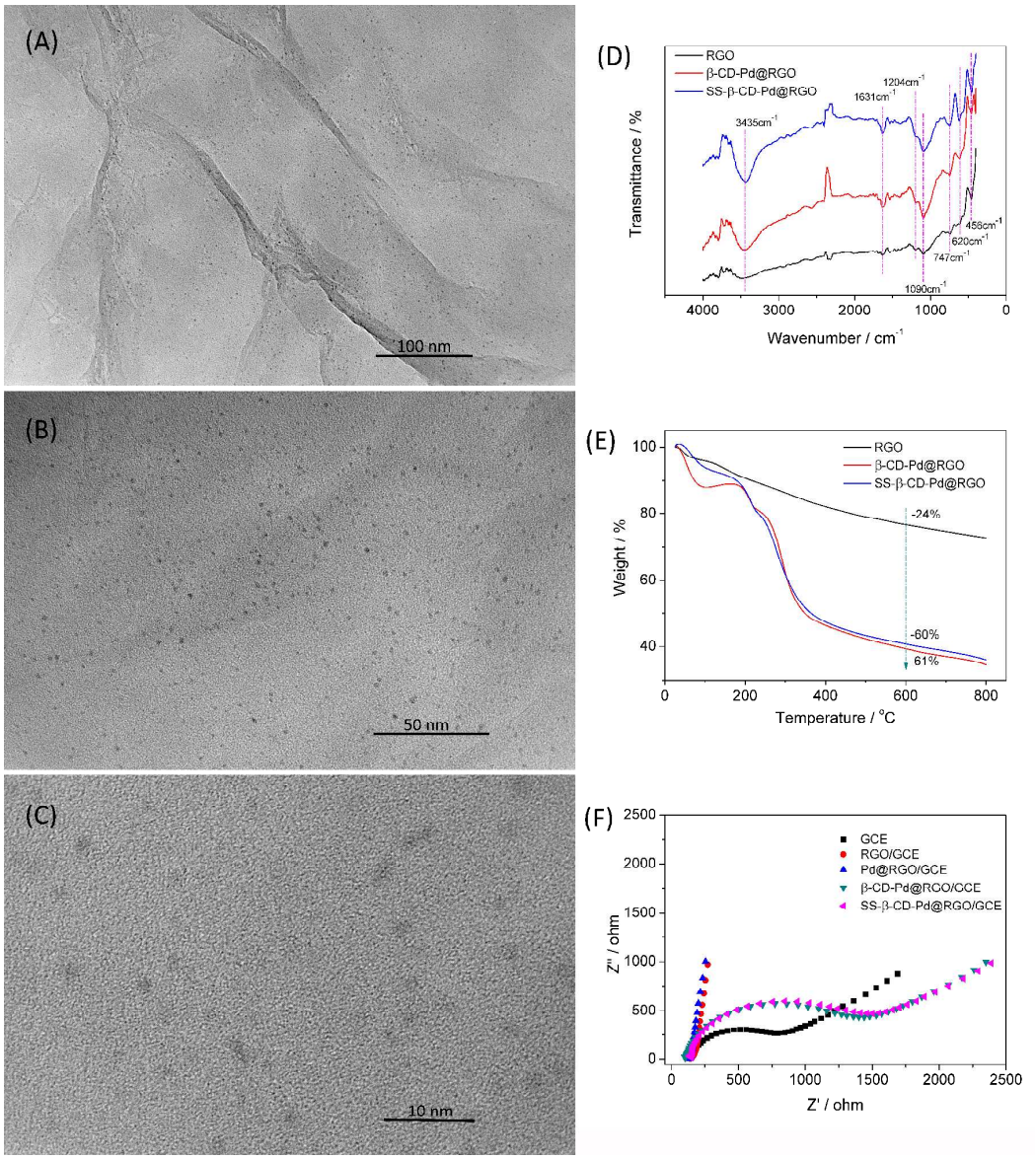

Fig.2

Ran et al.

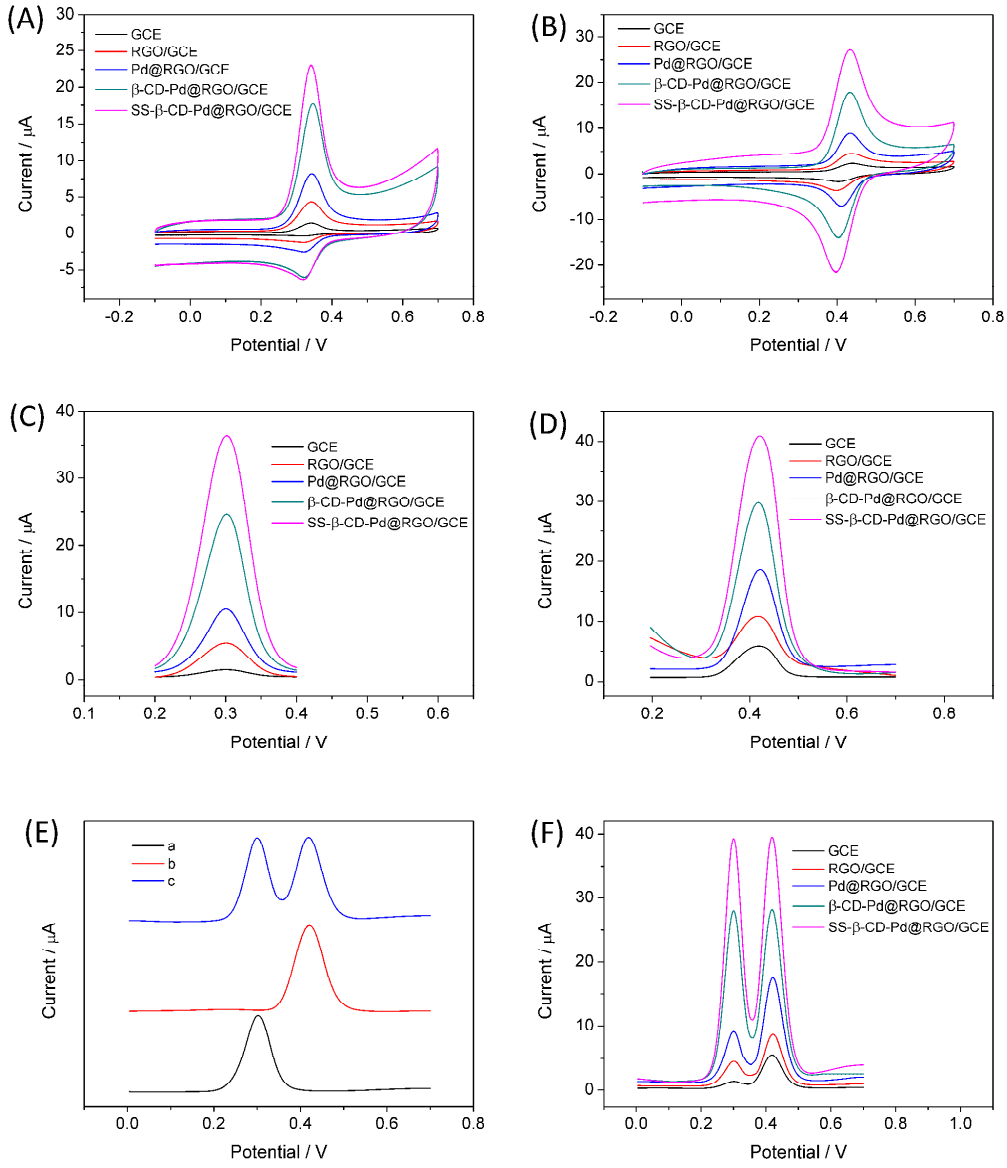

Fig. 3

Ran et al.

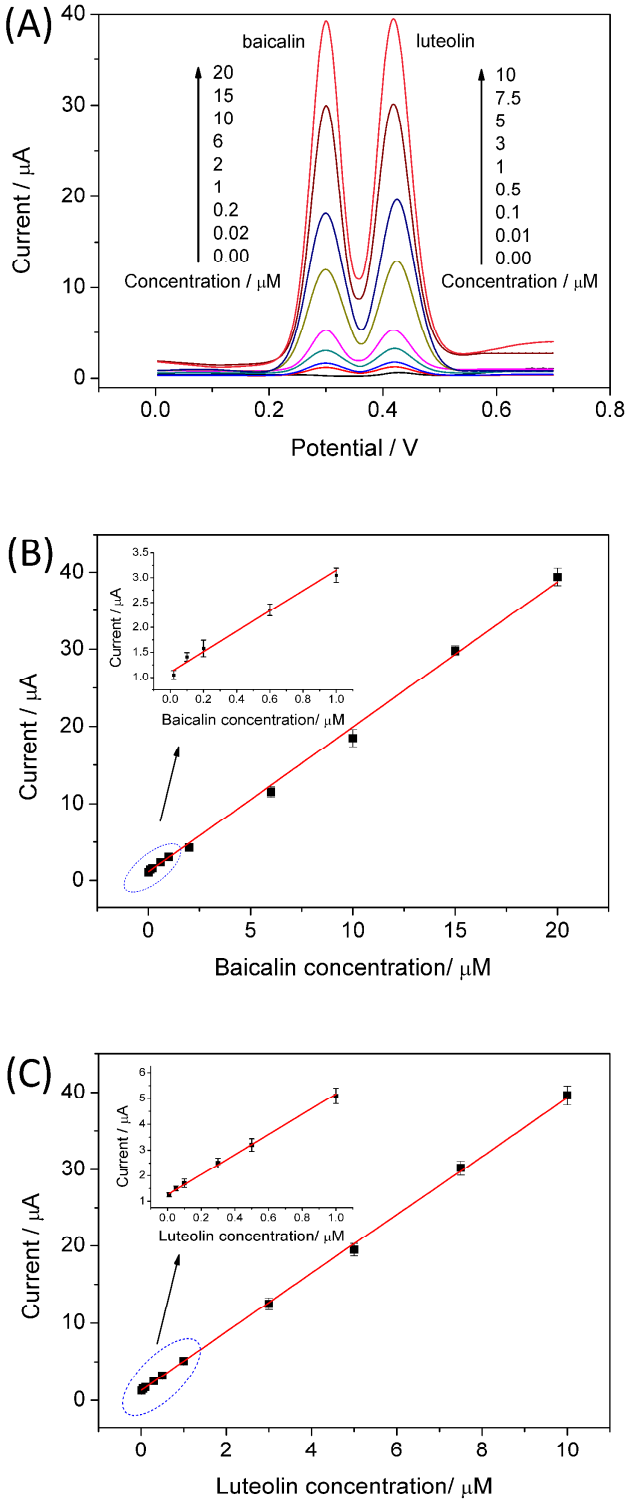

Fig. 4

Ran et al.

Table 1

Comparison of the analytical parameters for baicalin and luteolin detection by different electrodes.

Sample	Electrode	Method	Liner range (μM)	LOD (μM)	Ref
baicalin	Carbon disc electrode	CE-ED	1.0–1000	0.548	60
	DM-β-CD-GNs/GCE	DPV	0.04–3.0	0.01	18
	SS-β-CD-Pd@RGO/GCE	DPV	0.02–20	0.007	This work
luteolin	PDDA-G-CNTs/β-CD/GCE	DPV	0.05–60	0.02	61
	Carbon disc electrode	SWV	0.004–1.0	0.001	17
	GNs/HA/GCE	DPV	0.02–10	0.01	19
	SS-β-CD-Pd@RGO/GCE	DPV	0.01–10	0.0052	This work

Table 2

Determination of baicalin and luteolin in human serum samples (*n*=3).

Sample	Added (μM)		Founded (μM)		RSD (%)		Apparent recovery (%)	
	baicalin	luteolin	baicalin	luteolin	baicalin	luteolin	baicalin	luteolin
1	1.0	0.5	1.02	0.53	4.5	5.6	102.0	106.0
2	10.0	5.0	9.84	4.83	3.9	4.5	98.4	96.6
3	15.0	7.5	15.53	7.41	3.1	2.9	103.5	98.8

Tables

Ran et al.

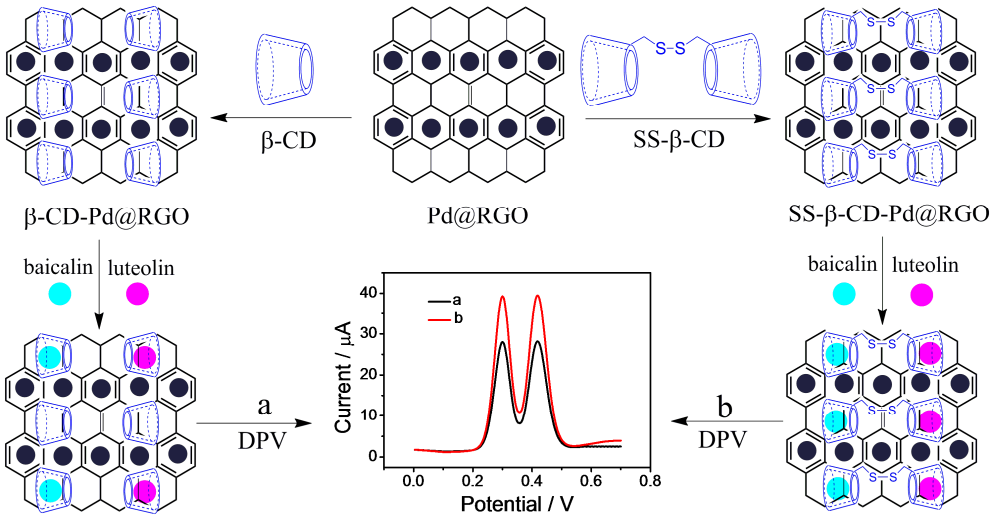

Graphic Abstract

The illustration of the SS-β-CD-Pd@RGO nanohybrids simultaneously sensing baicalin and luteolin by an electrochemical strategy.